nature energy

ARTICLES

PUBLISHED: 11 JANUARY 2016 | ARTICLE NUMBER: 15009 | DOI: 10.1038/NENERGY.2015.9

Fast and reversible thermoresponsive polymer switching materials for safer batteries

Zheng Chen[1], Po-Chun Hsu[2], Jeffrey Lopez[1], Yuzhang Li[2], John W. F. To[1], Nan Liu[1], Chao Wang[1], Sean C. Andrews[1], Jia Liu[1], Yi Cui[2]* and Zhenan Bao[1]*

Safety issues have been a long-standing obstacle impeding large-scale adoption of next-generation high-energy-density batteries. Materials solutions to battery safety management are limited by slow response and small operating voltage windows. Here we report a fast and reversible thermoresponsive polymer switching material that can be incorporated inside batteries to prevent thermal runaway. This material consists of electrochemically stable graphene-coated spiky nickel nanoparticles mixed in a polymer matrix with a high thermal expansion coefficient. The as-fabricated polymer composite films show high electrical conductivity of up to 50 S cm^{-1} at room temperature. Importantly, the conductivity decreases within one second by seven to eight orders of magnitude on reaching the transition temperature and spontaneously recovers at room temperature. Batteries with this self-regulating material built in the electrode can rapidly shut down under abnormal conditions such as overheating and shorting, and are able to resume their normal function without performance compromise or detrimental thermal runaway. Our approach offers 10^3–10^4 times higher sensitivity to temperature changes than previous switching devices.

Reliable and high-performance lithium-ion batteries (LIBs) are highly desirable for consumer electronics, electrical vehicles and grid energy storage[1–3]. Whereas the energy density, power density and cycling life of LIBs have been significantly improved in the past two decades, battery safety remains an important and unresolved issue. A high battery specific energy density generally increases the energetic response when the batteries are subjected to abuse. Safety issues have become a major obstacle impeding the large-scale application of high-energy-density LIBs.

To ensure good performance, LIBs generally operate within a limited range of current density, voltage and temperature[4]. However, at an abnormal temperature (for example, >150 °C), typically caused by shorting, overcharging or other abuse conditions, a series of exothermic reactions can be initiated and rapidly propagate to further increase the internal cell temperature and pressure, which results in catastrophic battery explosion and fire[5,6]. Commercial LIBs are equipped with external pressure release vents and positive temperature coefficient (PTC) resistors on their cases to prevent overpressure and overheating. However, pressure and temperature increases inside cells can occur at much higher speeds than can be detected by these external devices[7]. Thus, internal safety strategies are more effective in preventing thermal runaway.

There have been considerable efforts to design internal functional components to address battery safety issues, including novel separators, electrolyte additives and PTC-modified current collectors. Several novel separator approaches, including bilayer or trilayer separators[8,9], thermoresponsive microspheres[10] and ceramic particle coating[11,12], are effective in shutting down batteries or improving their thermal tolerance. However, the process is irreversible and the battery is no longer functional afterwards. On the other hand, electroactive polymer separator coatings for overcharge protection have limited operating voltages[13–15]. Additives (for example, flame retardants[16,17], redox shuttles[18–21]) to electrolytes still need to improve their operating voltage range and cycling stability. Non-flammable or solid-state electrolytes can avoid volatile solvents, although the battery performance is generally decreased owing to their low ionic conductivity[22–29]. PTC-modified current collectors are a promising approach owing to their simplicity and reversible operation. However, their application has been limited by low room-temperature conductivity and a considerable leakage current[7,30]. Other approaches such cathode doping[31] and electrode coating[32] have also led to some improved safety properties in certain conditions. Clearly, in spite of efforts made thus far, battery safety remains an important concern, thus calling for new approaches.

Here, we report fast and reversible thermoresponsive polymer switching (TRPS) incorporated internally into electrodes. Our material consists of conductive graphene-coated spiky nanostructured (nano-spiky) nickel particles as the conductive filler and a polymer matrix with a large thermal expansion coefficient. The nano-spikes on the particle surface enable a high electrical conductivity (σ) at a low filler fraction and a high thermal sensitivity, which is not possible with conventional spherical fillers such as carbon black (CB) or metal particles. The graphene coating stabilizes the metal particle surface, providing high electrochemical stability towards oxidation and electrolyte decomposition. The as-fabricated polymer composite films show values of σ of up to 50 S cm^{-1} at room temperature, about 10^2 times higher than common conductive polymer composites. The value of σ decreases in less than a second by seven to eight orders of magnitude on approaching the transition temperature and returns to high conductivity after cooling. Our TRPS device is 10^3–10^4 times more sensitive to temperature change than previous switching devices. Batteries with this internally incorporated TRPS show excellent cell function in a wide voltage window at normal temperature, and rapid shut-down at abnormal conditions (for example, overheating, shorting). They can also resume normal function repeatedly without

[1]Department of Chemical Engineering, Stanford University, California 94305, USA. [2]Department of Materials Science and Engineering, Stanford University, California 94305, USA. *e-mail: yicui@stanford.edu; zbao@stanford.edu

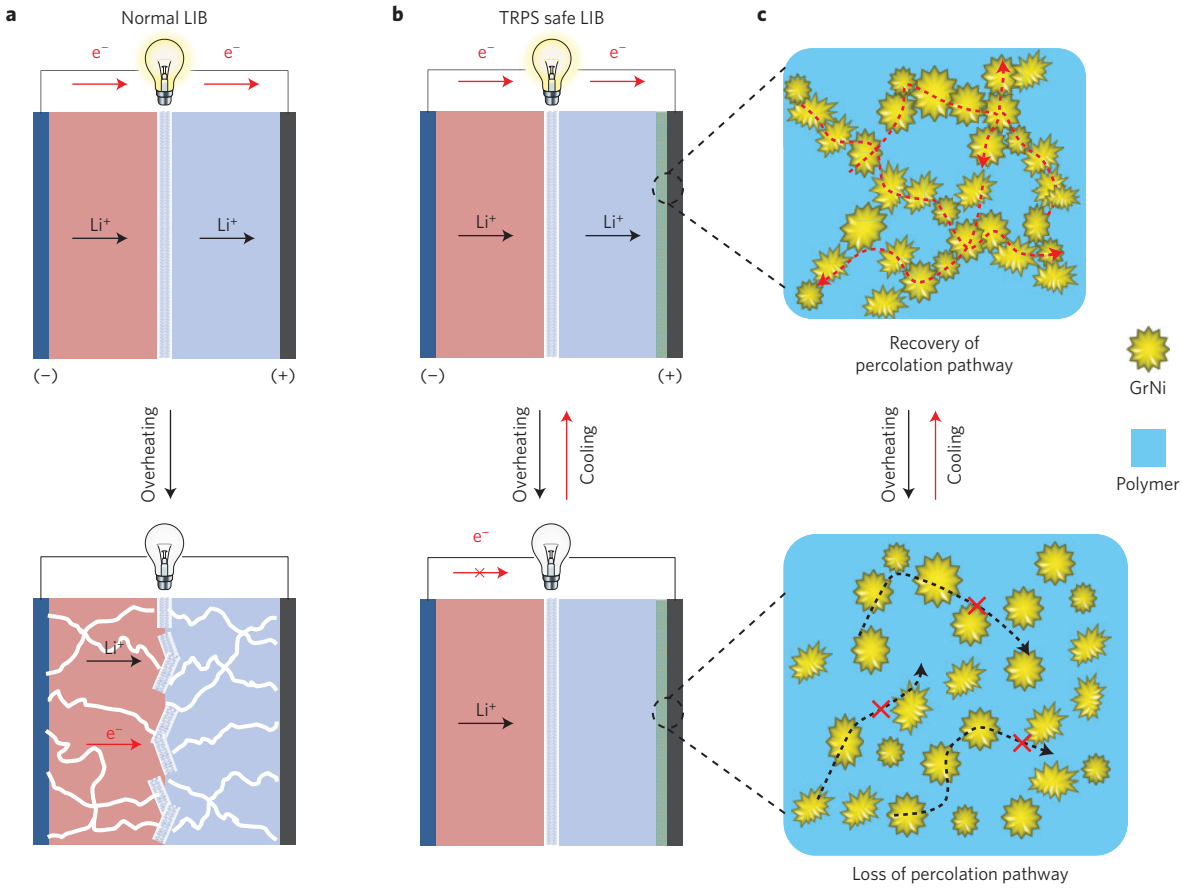

Figure 1 | Schematic illustration of safe battery design. a, A normal LIB consists of an anode (for example, graphite coated on Cu), a separator (for example, porous polyolefin), a cathode (for example, $LiCoO_2$ coated on Al) and a flammable electrolyte. On abnormal heating, the separator will melt, resulting in internal shorting of the battery. The marked increase in temperature will cause thermal runaway and permanently damage the battery structure. **b**, The safe battery has one or two current collectors coated with a thin TRPS layer. It operates normally at room temperature. However, in the case of a high temperature or a large current, the TRPS will be activated, greatly increasing its resistance and shutting down the battery. The battery structure can thus be protected without damage. **c**, Thermal switching mechanism of the TRPS material. The polymer composite film has a high electrical conductivity at room temperature due to the quantum tunnelling effect enabled by the spiky nanostructure (GrNi). On heating, the polymer matrix expands, thus separating the conductive particles, which can decrease the value of σ by a factor of 10^7–10^8. On cooling, the polymer shrinks and regains the original conductive pathways. The symbol (×) illustrates blocking of electron or ion transport.

performance compromise even after multiple overheating events. This is the first time that an approach has provided a combination of reliability, fast response time, and reversibility without sacrificing battery performance.

Safe battery design

A typical LIB comprises a flammable organic electrolyte and electrode materials (often metal oxides), which are separated by a porous polyolefin separator with a melting point (T_m) of ~130 to 160 °C (ref. 9). Such a battery is typically operated under a large cell voltage (~3.5–4.2 V) that exceeds the thermodynamic stability window[8]. When a large amount of heat is generated by shorting or overcharging, the battery separator will melt, which triggers and accelerates exothermic reactions between two electrodes and the electrolyte, leading to the catastrophic 'thermal runaway'[8] (Fig. 1a).

Our safety concept is demonstrated in Fig. 1b. In this design, a TRPS layer is added to at least one of the current collectors (here we use the cathode as an example) to form a hybrid current collector. As further illustrated in Fig. 1c, our proposed TRPS film is based on a modified quantum tunnelling composite (QTC) made from nanostructured metal particles with a graphene coating as the filler and a polymer with a high thermal expansion coefficient (for example, semi-crystalline polymer) as the matrix. The nanostructures on the surface of the metal particles are essential as high σ can be obtained on this QTC-based TRPS film at normal operating temperatures (for example, <60 °C) owing to the enhanced electrical tunnelling due to the nano-spikes. Such a tunnelling effect can provide a much higher local electrical field at the nano-spikes than that at the surface of regular spherical particles, thus enhancing the conductive percolation[33]. The TRPS film instantaneously becomes insulating and shuts down the battery above its switching temperature (T_s) as a result of volume expansion of the polymer matrix that separates the conductive particles and breaks the conductive pathways[34]. When the temperature cools to below T_s, the TRPS film contracts and recovers its high σ. Because the conductivity change of the TRPS film is reversible, the battery can be repeatedly shut down and revived.

One attractive feature of this approach is that the T_s value of TRPS can be rationally designed to meet the requirement of a desirable battery operating temperature by adjusting its composition. In real battery modules, the TRPS can also be used to monitor the internal temperature of a battery and allow an external control system to take action to further protect batteries. Once the normal temperature is reached after intervention, the internal cell resistance returns to a small value and the battery can be operated again as usual. Such TRPS allows a fast and reversible shut-down of

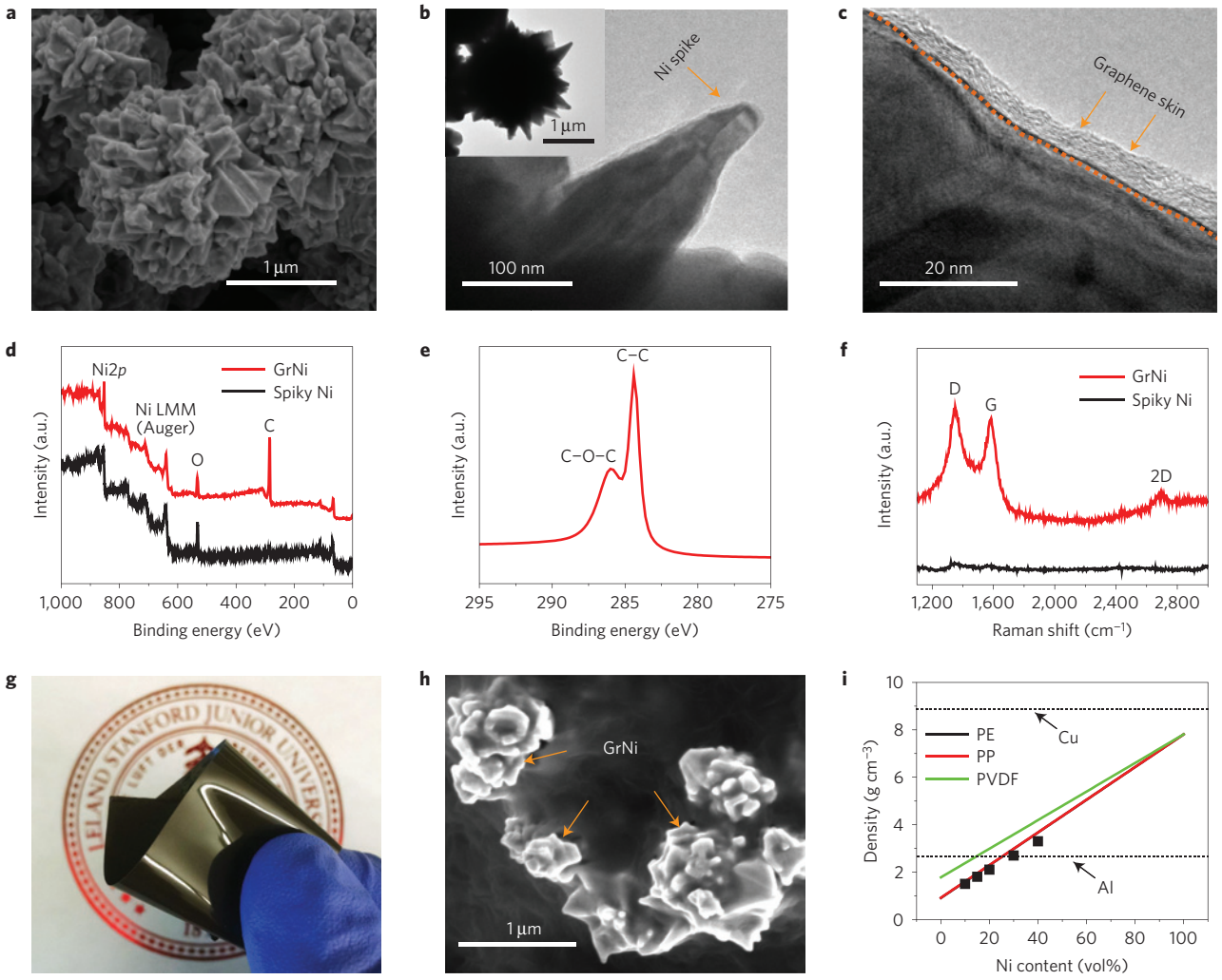

Figure 2 | Structure and composition of graphene-coated nano-spiky Ni and as-fabricated TRPS material. a, SEM image of GrNi particles. **b**, TEM image of a single Ni spike with a uniform graphene coating. The inset shows a GrNi particle with a typical nano-spiky structure. **c**, High-resolution TEM of the conformal graphene layer on GrNi with a thickness of 5–10 nm. **d**, XPS spectra of original spiky Ni and GrNi. **e**, C1*s* XPS spectrum peak of GrNi, indicating the graphene coating. **f**, Raman spectra of original spiky Ni and GrNi. The intense G peak and clear 2D peak of GrNi confirm the excellent graphene coating. **g**, Digital photograph of a freestanding TRPS film based on PE/GrNi with a 20 vol% GrNi loading. **h**, SEM image of the PE/GrNi-based TRPS composite showing the GrNi network embedded in the PE matrix. **i**, Dependence of the TRPS composite density on the GrNi volume fraction for different polymer matrices, including PE, PP and PVDF. Solid line, calculated density; squares, measured density. For comparison, the dashed straight horizontal lines indicate the densities of Cu and Al.

LIBs before dangerous events start, without structural damage to the battery or performance degradation.

Materials fabrication and characterization

As a model system, we first used graphene-coated nanostructured nickel (Ni) particles with spiky protrusions as the conductive filler and polyethylene (PE) as the polymer matrix to make QTC-based TRPS composite. The spiky nanostructures of Ni particles are essential because they amplify the charge transport by a field-assisted tunnelling effect and provide a high σ at low volume fraction[33]. However, Ni is subject to electrochemical oxidation at high voltage (for example, >4 V versus Li/Li$^+$) and promotes electrolyte decomposition[35,36]. To solve this problem, graphene-coated nano-spiky Ni particles (GrNi) were synthesized (see Methods) to provide a stable Ni–electrolyte interface. Scanning electron microscopy (SEM, Fig. 2a) and transmission electron microscopy (TEM, Fig. 2b) images show that the GrNi particles maintain the spiky nanoscale surface features, similar to the native Ni (Supplementary Fig. 1). The size of GrNi particles mainly ranges from 1 to 3 µm. A graphene skin is conformally formed on the surface of Ni with a typical thickness of 5–10 nm (Fig. 2c). X-ray photoelectron spectroscopy (XPS) further confirms the coating of graphene on the surface from the intensive C1*s* peak (Fig. 2d,e). Raman spectroscopy (Fig. 2f) shows a sharp G peak (~1,580 cm^{-1}) and a clear 2D peak (~2,670 cm^{-1}), further confirming the excellent graphene coating. Such a dense graphene coating is required to provide good electrochemical stability in battery cycling while maintaining a high electrical conductivity.

PE is selected as the matrix polymer as it is one of the major components in commercial separators and is electrochemically stable in LIBs. Its high thermal expansion coefficient ($\alpha \sim 10^{-4}$ K^{-1}) is important to realize a fast response to temperature change. Here we use low-density PE (LDPE) because its melting temperature (T_m) (Supplementary Fig. 2) is lower than that of the high-density PE used for the LIB separators. This will allow the battery to shut down before the temperature becomes high enough to damage the separator. Other polymers, such as polypropylene (PP) or polyvinylidene fluoride (PVDF), are also viable for our

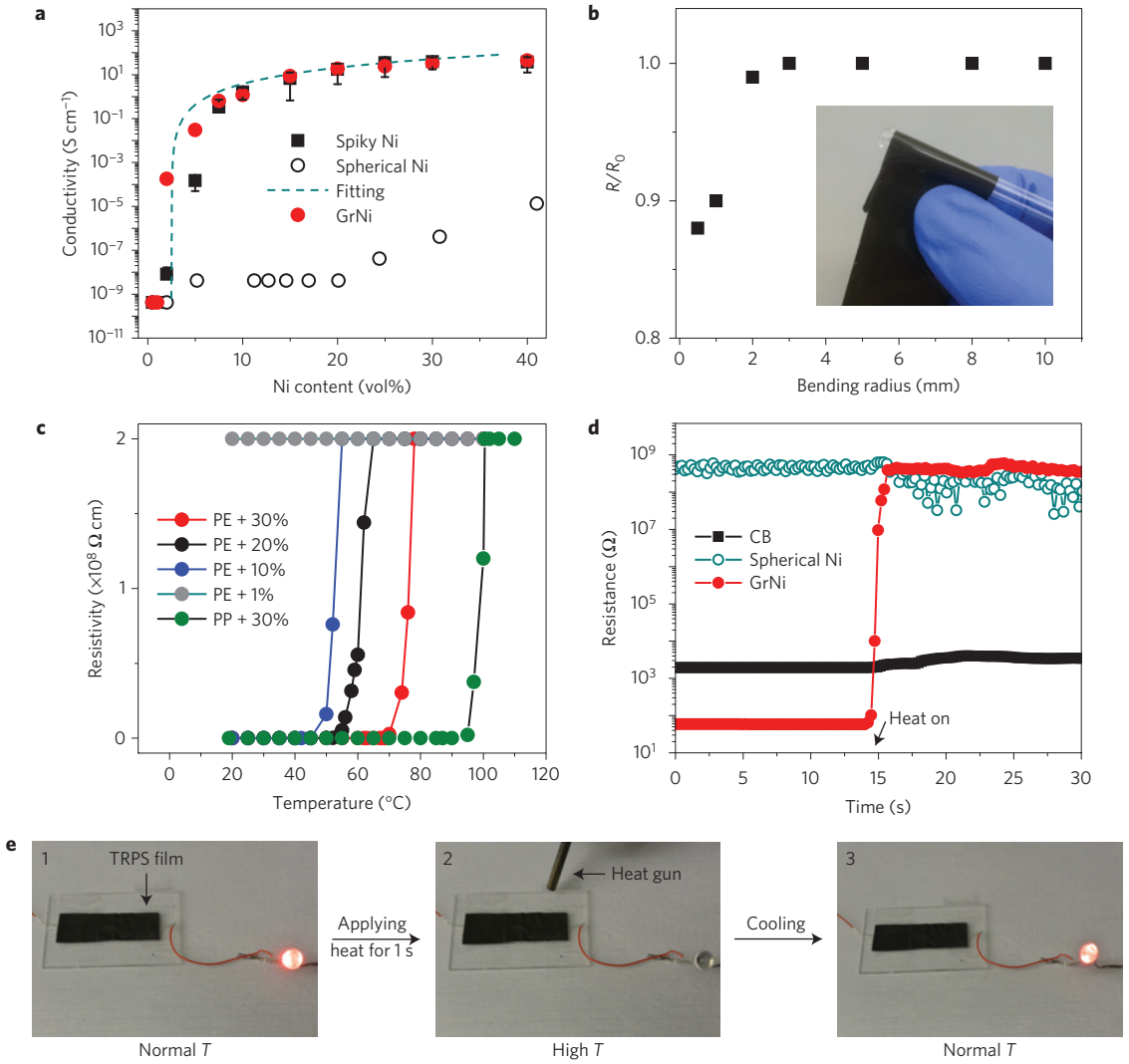

Figure 3 | Physical properties of TRPS film. a, TRPS film conductivity as a function of the volume fraction for different conductive particle fillers (spiky Ni, GrNi and spherical Ni). Error bars represent the standard deviation from five samples per volume fraction. The dashed curve represents the best-fit line for conductivity above the percolation threshold using percolation theory. **b**, Dependence of the relative resistance of a freestanding TRPS film (~50 μm) on its bending radius. Inset shows the TRPS film rolled on a glass tube with a diameter of 4 mm. **c**, Resistivity changes of different TRPS films as a function of temperature, including PE/GrNi with different GrNi loadings and PP/GrNi with a 30 vol% loading of GrNi. The resistivity of PE/GrNi with a 1 vol% loading of GrNi remained large at 20–90 °C owing to an insufficient number of conductive pathways. **d**, Dependence of resistance on time for PE-based composites with different conductive fillers on heating. The resistance of PE/GrNi increased by 10^8 in <1 s. **e**, Demonstration of thermal switching behaviour of a TRPS film using a LED connected in the circuit.

design, potentially offering different T_s. QTC-based TRPS current collectors were then fabricated by uniformly blending the GrNi with molten PE and casting a homogeneous thin film (20 μm or less) on Cu, Al or other substrates (Supplementary Fig. 3).

Freestanding TRPS films can be readily obtained by carefully peeling off from a non-adhesive substrate (for example, glass). Fig. 2g shows an example of a PE/GrNi film (20 vol% of Ni) under folding and twisting, indicating its excellent mechanical flexibility. The SEM image (Fig. 2h) clearly reveals the spiky GrNi particle network embedded in the PE matrix, forming conductive pathways. Owing to the intrinsic low density of PE ($\rho_{PE} \sim 0.93\,g\,cm^{-3}$), the measured bulk density of PE/GrNi remains low even with a large fraction of GrNi, for example, 2.9 g cm^{-3} at 20 vol% of GrNi (Fig. 2i). Such a density is close to Al (2.7 g cm^{-3}) and much lower than Cu (8.96 g cm^{-3}), thus making it desirable for lightweight electrode applications.

The PE/GrNi-based TRPS composites show a high σ with a relatively low loading of GrNi particles. As shown in Fig. 3a, the dependence of conductivity on Ni volume fraction follows the percolation theory, with a percolation threshold of ~0.02, which agrees with previous studies on various nanostructured conductive composites[37]. The value of σ can reach as high as ~50 S cm^{-1} at a 40 vol% GrNi loading. The σ values of previous CB-based PTC composites are in the range from 0.01 to 1 S cm^{-1} (refs 7,38–40), significantly lower than our TRPS composites. Composites made from native spiky Ni can reach similar conductivities at high Ni loadings yet the percolation threshold (0.05) is slightly higher than PE/GrNi. This might be due to improved dispersion and reduced aggregation of GrNi in the nonpolar PE at low volume fraction due to the graphene coating. By comparison, using smooth spherical Ni particles (Supplementary Fig. 4) as the conductive filler gives composites showing very low σ even with a high Ni loading, confirming the important role of spiky nanostructures on the Ni surface. The σ of the PE/GrNi film remains stable at a normal bending radius, which further confirms its excellent mechanical properties (Fig. 3b); σ is reduced by ~10% as the bending

radius decreases to 0.5 mm, possibly owing to the deformation of the PE matrix, which slightly decreases the local particle-to-particle distances.

The σ of PE/GrNi changes rapidly as the temperature approaches T_s. Figure 3c shows the resistivity dependence on temperature for different TRPS films. Taking PE/GrNi with 30 vol% of GrNi as an example, the resistivity increases by ~8 orders of magnitude as the temperature steadily goes from 20 to 80 °C. This corresponds to a rate of change of resistivity of $\sim 4 \times 10^7\ \Omega\ cm\ °C^{-1}$ at T_s (65–70 °C). Such a resistivity change is 10^3–10^4 times higher than previous PTC composites used for LIB, such as poly(methyl methacrylate) (PMMA)/CB (ref. 39), PE/CB (ref. 41) and epoxy/CB (ref. 7). The huge resistance change of TRPS films can be attributed to the quantum tunnelling effect between spiky GrNi particles associated with the volume expansion of PE below the T_m (ref. 42).

The T_s of different PE/GrNi compositions can be tuned by adjusting their ratios. For example, the T_s of PE/GrNi with 20 and 10 vol% of GrNi decreased to ~58 and ~50 °C, respectively. Differential scanning calorimetry (DSC) measurements (Supplementary Fig. 5) show that the T_m of PE/GrNi remains similar (~95 °C) for different compositions, thus confirming that the change of σ is due to the nonlinear volume expansion of PE below T_m. Similarly, the T_s can be further enhanced using polymers with higher T_m, such as PP at ~150 °C (Supplementary Fig. 6) and PVDF at ~170 °C (Supplementary Fig. 7). By choosing different polymers, and further controlling their ratio, the T_s of TRPS films can be tuned over a wide range of temperatures to meet various applications[4,43].

The thermally induced switching of our TRPS film is very fast and highly reversible. As shown in Fig. 3d, on directly heating to ~80 °C, the resistance of a PE/GrNi (20 vol% of GrNi) film increased from ~2 to $\sim 10^8\ \Omega$ in less than 1 s. When the film was cooled to 25 °C, the resistance decreased back to between 2 and 5 Ω. This thermal switching behaviour is reversible over repeated heating and cooling cycles. After 20 switching cycles, the polymer film still retained good conductivity at room temperature and showed high resistivity at high temperature (Supplementary Fig. 8). By comparison, the resistance of a PE/CB film with the same composition increased from ~2,000 to only 5,000 Ω in 5 s at the same heating condition. Figure 3e further demonstrates the efficient thermal switching behaviour of PE/GrNi. A LED was connected to a TRPS film in the circuit and lights up at room temperature. The LED is shut off soon after applying heat with a hot air gun. After removal of the hot air gun, the polymer film cooled down and LED lit up again. The shut-down response time is less than 1 s (Supplementary Video 1) on applying the heat source, confirming an ultrafast switching behaviour. Such a fast response is especially important for battery safety control.

Safe battery performance and switching behaviour

To demonstrate the function of TRPS film in batteries, we used TRPS-film-coated current collectors (Fig. 4a). For example, a PE/GrNi (20 vol% GrNi) film with a thickness of ~15 μm was coated on a 20 μm Al foil (Fig. 4b). Because the film can be easily sliced (Supplementary Video 2), a conventional electrode fabrication process can be readily used. $LiCoO_2$ was then coated onto the TRPS current collector as working electrodes to assemble batteries using lithium as the anode (Fig. 4c). Cyclic voltammetry curves of TRPS film made from native spiky Ni showed large oxidation and reduction (mainly due to the surface oxide layer) currents from side reactions (Fig. 4d), agreeing with previous reports[35,36]. By comparison, PE/GrNi showed negligible current from 0.01 to 4.7 V (versus Li/Li^+), indicating the excellent electrochemical stability provided by the graphene coating. Full cells made from $LiCoO_2$ and graphite using GrNi-based TRPS film show much higher Coulombic efficiency and cycling stability than those using native Ni particles, further confirming the importance of the graphene coating (Supplementary Fig. 9). The TRPS film resulted in a slightly increased Ohmic resistance in the safe batteries compared with the normal ones (Fig. 4e). Nevertheless, the total cell equivalent series resistance (ESR) decreased slightly, possibly owing to improved electrochemical contact on the electrodes and interfaces with the elastic TRPS layer.

Such batteries can be operated in a similar way to normal batteries without sacrificing electrochemical performance. As shown in Fig. 4f, at room temperature no clear difference was observed between safe and normal batteries in the galvanostatic charge/discharge cycling, indicating good electrochemical stability of the safe batteries (Supplementary Fig. 10). The rate capability of safe batteries is slightly better than normal batteries (Supplementary Fig. 11), which is consistent with the electrochemical impedance spectrum (EIS) measurements. Similarly, safe cells based on graphite anodes also showed similar cycling performance to those of normal cells at room temperature, further suggesting good electrochemical stability at a low potential (Supplementary Fig. 12). Moreover, the safe batteries can be operated stably at moderate temperature (20–50 °C). To better evaluate the intrinsic thermal stability of TRPS film, we used $LiFePO_4$ as the active material to perform cycling at 50 °C. As shown in Supplementary Fig. 13, the safe battery with TRPS film can be cycled with similar stability to that of a normal battery, indicating its good thermal tolerance. These results suggest that the TRPS film is highly compatible with the current LIB chemistry and meets the key requirements for real battery operation.

Batteries with TRPS film respond rapidly to overheating. As shown in Fig. 4g, a safe $LiCoO_2$ battery was initially cycled stably at 25 °C; once the temperature was increased to 70 °C, it immediately shut down owing to the rapid increase of the ESR (Supplementary Fig. 14). After cooling to 25 °C, the battery can resume normal cycling starting from the previous shut-down potential. The retention of an open-circuit potential indicates a negligible leakage current after shut-down. This thermal switching process can be reproduced multiple times on the same battery (Supplementary Fig. 15). As summarized in Fig. 4h, the safe battery delivered a stable capacity at room temperature, with little degradation during cycling, whereas the cycling capacity dropped to almost zero at high temperature, further indicating a highly reversible shut-down process. Similar thermal switching behaviour was also observed for safe graphite batteries (Supplementary Fig. 16), on which repeated shut-down and recovery can also be realized. Considering that the volume expansion of various PE in the temperature range of 0–80 °C is <10% (ref. 33), the thickness of a TRPS film is about 15 μm, and the overall thickness of a single-cell battery is >100 μm, the total thickness change of the TRPS film (<1.5 μm) has a trivial effect on the whole battery structure, thus ensuring stable operation during repeated thermal cycling.

Mechanistic understanding

The most common reasons causing battery thermal runaway are overheating and shorting[5]. The above results have shown the efficacy of our TRPS film towards protecting battery overheating. There have been several reports about internal PTC devices for safe battery application. However, all of them used CB as the conductive filler[7,30,39,44,45], which results in an approximately 10^2 times higher initial resistance than our graphene-coated spiky Ni-based TRPS composite. This will invariably compromise the battery performance under normal operating conditions. They also showed a significant leakage current due to the much smaller resistivity increase (10^2–10^4 versus 10^8 times) than our TRPS film at T_s, meaning that they cannot fully shut down a failing battery. We also note that spherical Ni particles have been used together with CB to make PTC devices[30]; however, the electrode instability issue and small resistance change remained to be solved. Our surface-stabilized nano-spiky Ni particle filler endows the TRPS

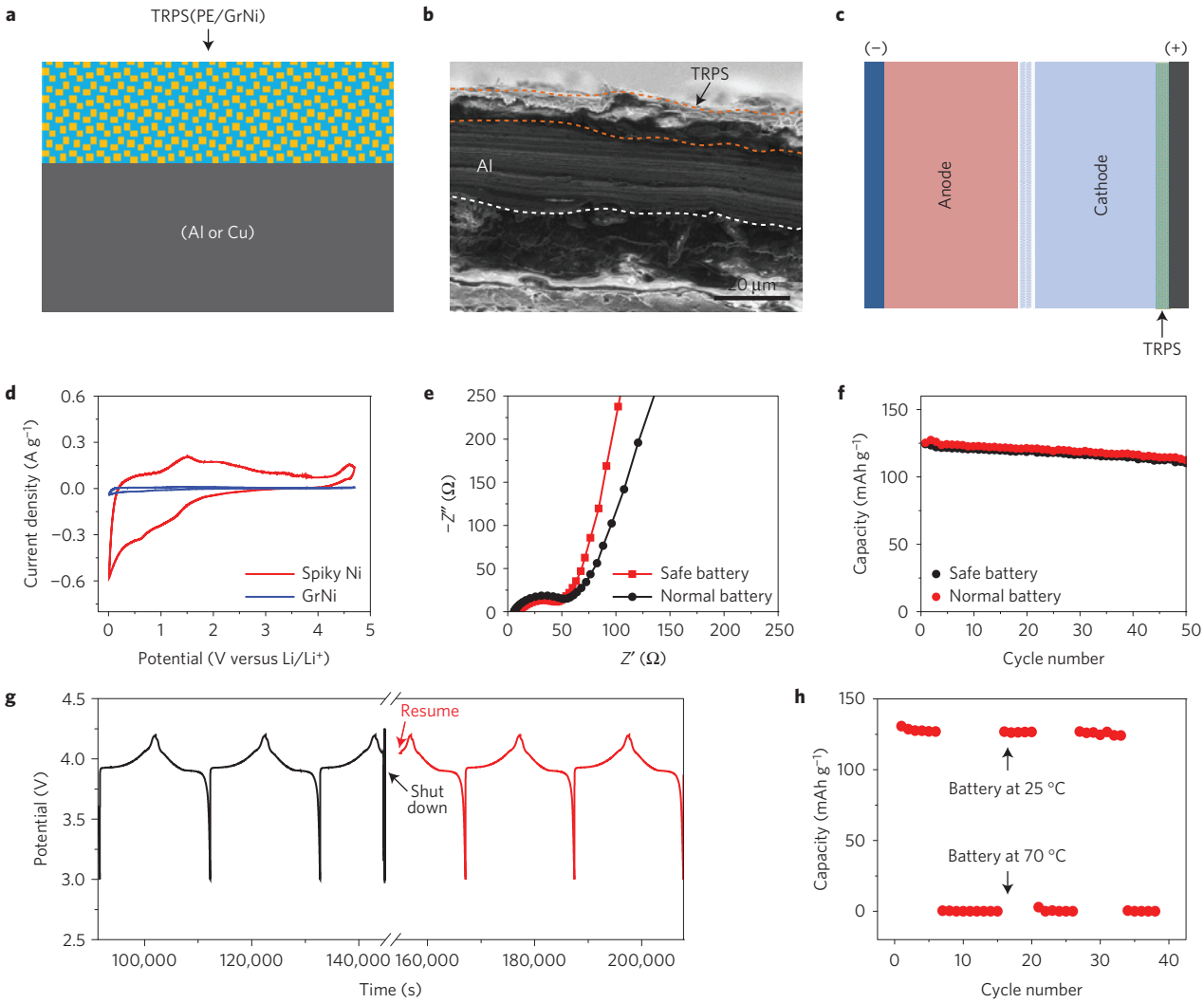

Figure 4 | Battery performance. a, Schematic illustration of TRPS-film-coated current collectors. The composite can be coated on various substrates with good adhesion. **b**, SEM image of a PE/GrNi thin film (~15 μm, 20 vol% GrNi) coated on an Al current collector (20 μm). **c**, Schematic illustration of a safe battery based on the TRPS-film-coated Al as current collector, $LiCoO_2$ as cathode and lithium as anode. **d**, Cyclic voltammetry curves of original spiky Ni and GrNi (1 mg cm^{-2}) in the potential window of 0.01–4.7 V (versus Li/Li^+). The GrNi shows a much smaller current from undesired side reactions. **e**, Electrochemical impedance spectra of normal and safe $LiCoO_2$ batteries at open-circuit voltage. **f**, Cycling behaviour of normal and safe $LiCoO_2$ batteries at 25 °C in the potential window of 3.0–4.3 V. They show similar specific capacities (~125 mAh g^{-1}) and capacity retention (~95% after 50 cycles), indicating the excellent electrochemical stability of the PE/GrNi on the cathode side. **g**, Safe $LiCoO_2$ battery cycled at a charge or discharge in 3 h followed by rapid shut-down on overheating (70 °C). The charge/discharge voltage profile is similar to a typical $LiCoO_2$ battery. After cooling to 25 °C, the same battery resumes its normal cycling. No obvious change can be observed from the voltage profile. **h**, Capacity summary of the safe $LiCoO_2$ battery cycling between 25 °C and shut-down. The near-zero capacity at 70 °C indicates full shut-down.

film with a high conductivity at low temperature, a high tolerance to electrochemical oxidation, a large resistance increase at T_s, and a short response time (<1 s) to shut down failing batteries.

An experimental demonstration of shorting protection by TRPS film is limited by our capability to build large-sized batteries, as these are needed to generate sufficient heat on shorting. Nevertheless, simulation of a battery thermal behaviour with a capacity of 2,000 mAh suggests that shorting-induced thermal runaway can be prevented by our TRPS film. To further understand the thermal switching, we performed a COMSOL simulation to monitor the change of battery temperature on nail shorting (see Methods). As shown in Fig. 5a, a battery with ten laminates is shorted by a nail from the centre of the case. Batteries with and without a TRPS current collector show markedly different thermal behaviours (Fig. 5b).

For normal batteries, nail shorting can lead to fast electrochemical reactions and generate a large amount of heat that can increase the battery temperature rapidly. As shown in Fig. 5b,c, the internal temperature of a normal LIB can increase to above 300 °C in 60 s. This is close to *in operando* observation of thermal runaway in real batteries using high-speed tomography[6]. In the safe batteries, besides electrochemical reactions, a large current passing through the TRPS film under shorting can also increase the temperature through Joule heating, which can quickly activate the thermal switching and shut down the current flow. This will terminate the battery reactions and prevent thermal runaway. By applying the dependence of resistance on temperature (Fig. 3c and Supplementary Fig. 7), batteries with different TRPS films show similar thermal responsive behaviour (Fig. 5b,c). The temperature of all the safe batteries increased to their T_s and remained stable owing to shut-down. For example, the PE/GrNi-based safe battery reaches a maximum temperature of only 70 °C on shorting before it automatically shuts down. Although our simulation is based

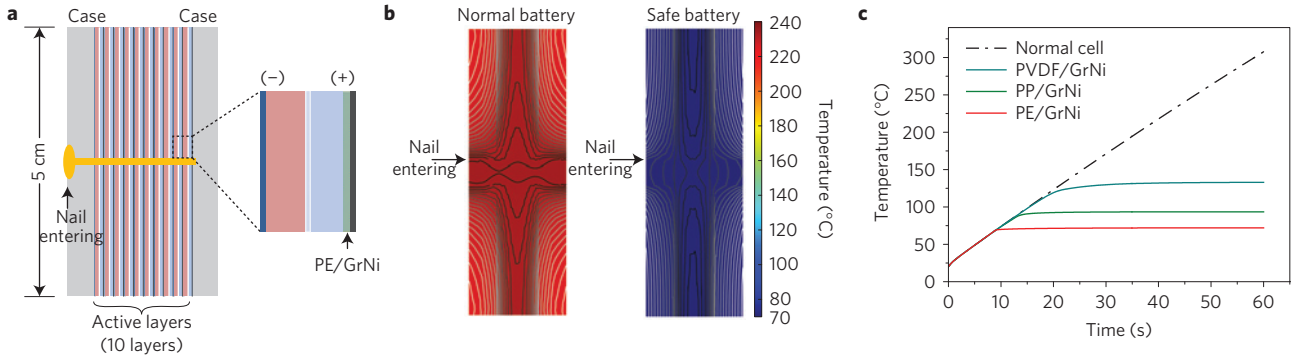

Figure 5 | COMSOL simulation of battery behaviour after nail shorting. a, Schematic illustration of the battery structure (experimental section, Supplementary Information) used for thermal modelling. The nail is placed in the centre of the case. For the normal cell, the current collectors are Al (cathode) and Cu (anode). For the safe battery, the current collector is TRPS-film-coated Al or Cu. **b**, Two-dimensional temperature profiles on the cross-section of normal and safe batteries after shorting for 30 s. The arrows show the position of the nail on each cell. **c**, Battery temperature dependence on shorting time. The normal battery and the safe batteries show significantly different thermal behaviour.

on relatively simple conditions, the clear trend and significantly different thermal behaviour between normal batteries and safe batteries suggest the great promise of using designed TRPS films to control battery safety under various failure conditions.

It is also noted that, with the increased size and thickness of a battery, the external heat propagation into the battery may not be fast enough to instantaneously trigger the shut-down with TRPS, and an ionic current could still flow. To develop more effective TRPS for real battery safety management, we expect that TRPS composites with very high thermal conductivity are needed. In addition, optimized cell structures that can accommodate the TRPS composite so as to respond to external stimuli more rapidly should also be designed.

Conclusion

In summary, we have developed a class of ultrafast, reversible TRPS materials for safer batteries. They are enabled by the use of graphene-coated nano-spiky Ni particles, which offer high σ at low particle fraction, high thermal sensitivity, and excellent electrochemical stability. The TRPS material shows excellent mechanical flexibility, a high room-temperature σ, a large operating voltage window, ultrafast thermal switching and a large decrease of σ on heating. These properties have not been achieved using previous polymer PTC devices. Safe batteries with this TRPS material show excellent battery performance at normal temperature and shut down rapidly under abnormal conditions, such as overheating and shorting. They can also resume normal function without compromising performance after intervention and repeated use. Compared with previous approaches, our design provides a reliable, fast, reversible strategy that can achieve both high battery performance and improved safety. Therefore, this strategy holds great promise for practical battery applications.

Methods

Synthesis of graphene-coated spiky Ni (GrNi). To make GrNi, ~5 g of spiky Ni particles (Novamet) were dispersed in 150 ml of triethylene glycol (TEG, Sigma Aldrich) and 500 µl of 50% w/w aqueous NaOH solution. After stirring at 185 °C for 8 h, the spiky Ni was collected by centrifugation and washed three times with ethanol. The NaOH solution facilitates decomposition of the organic solvent (TEG), allowing carbon atoms to diffuse into the Ni layer and adhere to the surface[46]. This primes the spiky Ni for low-temperature graphene growth. Samples were then dried in a vacuum oven at 50 °C for 1 h. The dried particles were placed in a tube furnace with the following temperature profile: heating to 100 °C at 2 °C min^{-1}; heating to 600 °C at 20 °C min^{-1}; holding temperature at 600 °C for 1 h. An Ar flow rate of 80 sccm was maintained throughout the ambient pressure annealing process.

Preparation of QTC switching polymer. The QTC-based TRPS films were fabricated by first mixing GrNi or native spiky Ni particles with polymers (for example, PE, PP) at different ratios under melting and then coating the mixture onto a substrate (for example, Al, Cu or glass). The PVDF-based TRPS film was made by dissolving PVDF in *N*-methyl-2-pyrrolidone (NMP) and dispersing Ni particles into the viscous polymer solution for film coating. Freestanding TRPS films were made by peeling off the coating layer from the glass substrate.

Battery fabrication and testing. Safe batteries were fabricated using TRPS-layer-coated Cu or Al film as the current collector. Cathode slurry was prepared by mixing active materials ($LiCoO_2$ or $LiFePO_4$), carbon black (CB) and PVDF at a mass ratio of 8:1:1 with NMP as the solvent. Anode slurry was prepared by mixing graphite, CB and PVDF at a mass ratio of 90:5:5. The working electrodes were fabricated by coating different slurries on various current collectors and dried in vacuum at 80 °C for 10 h. Half-cells were fabricated by sandwiching a working electrode, a separator (25 µm Celgard 2500) and a lithium disc. Full cells were made using a $LiCoO_2$ electrode (with or without TRPS films) as the cathode and a graphite electrode as the anode. The electrolyte was 1 M $LiPF_6$ in ethylene carbonate/diethylcarbonate (1:1 v/v). Cyclic voltammetry and EIS measurements were performed on a VMP3 potentiostat (Bio-Logic). Galvanostatic charge/discharge cycling was performed on BT 2000 test station (Arbin Instrument).

Thermal measurement. The room-temperature electrical conductivity was measured by the four-point probe method with a Keithley 4200. The PTC effect of various composites was tested using the two-terminal method by ramping and cooling samples in a temperature-controlled environmental chamber (ESPEC, model BTU-133), in which a digital multimeter (Amprobe CR50A) was connected to the samples. The safe battery cycling and switching test was also performed in the temperature chamber, with a temperature ramping rate of 2 °C min^{-1}. To measure the instantaneous thermal response of the polymer to heating, a hot air gun (X-Tronic 4000) set at 157 °C was used to heat the PTC film by blowing hot air. This allows the TRPS film temperature to reach ~80 °C immediately. The resistance change versus time was recorded by a precision LCR meter (Agilent E4980A).

COMSOL simulation. The internal-shorting-induced Joule heating behaviour of batteries was simulated by COMSOL Multiphysics 3.5a, using two-dimensional transient analysis of Heat Transfer and AC/DC modules. One normal cell contains a Cu foil, a graphite electrode, a separator, a $LiCoO_2$ electrode, and an Al foil. The battery is composed of ten unit cells sandwiched by ABS resin, and the centre is penetrated by a stainless steel nail. The safe batteries contain TRPS-coated current collectors. The battery is prismatic-type and has a total area of 500 cm^2 and a capacity of 2,000 mAh. Note that the simulation model does not contain the entire battery, but the size is large enough to demonstrate the thermal behaviour without losing generality. The Cu foil is grounded and the Al foil has an applied voltage of 3.7 V. The ambient air temperature is set as 20 °C and the heat transfer coefficient of the ABS–air interface is 10 W m^{-2} K^{-1}. The top and bottom boundaries are thermally insulated. When the battery is punctured by a steel nail, the positive and negative electrodes are shorted and inject all their current into the nail. The heating of the battery originates from the metal foils, the steel nail, and the internal resistance, which is evenly distributed among the graphite electrode, the separators and the $LiCoO_2$ electrodes. The internal resistance is assumed to be 0.075 Ω, and the ionic resistivity can be calculated to be 30 Ω m^{-1}, using the total area of the battery and the thickness of electrodes and separators. All the physical properties of the materials are listed in

Supplementary Table 1. For the time evolution of battery temperature, the probe position is located 1 mm above the steel nail along the centre line.

Received 15 August 2015; accepted 12 November 2015; published 11 January 2016

References

1. Dunn, B., Kamath, H. & Tarascon, J.-M. Electrical energy storage for the grid: a battery of choices. *Science* **334**, 928–935 (2011).
2. Choi, N. S. *et al.* Challenges facing lithium batteries and electrical double-layer capacitors. *Angew. Chem. Int. Ed.* **51**, 9994–10024 (2012).
3. Goodenough, J. B. & Park, K. S. The Li-ion rechargeable battery: a perspective. *J. Am. Chem. Soc.* **135**, 1167–1176 (2013).
4. Lu, L., Han, X., Li, J., Hua, J. & Ouyang, M. A review on the key issues for lithium-ion battery management in electric vehicles. *J. Power Sources* **226**, 272–288 (2013).
5. Wang, Q. *et al.* Thermal runaway caused fire and explosion of lithium ion battery. *J. Power Sources* **208**, 210–224 (2012).
6. Finegan, D. P. *et al. In-operando* high-speed tomography of lithium-ion batteries during thermal runaway. *Nature Commun.* **6**, 6924 (2015).
7. Feng, X. M., Ai, X. P. & Yang, H. X. A positive-temperature-coefficient electrode with thermal cut-off mechanism for use in rechargeable lithium batteries. *Electrochem. Commun.* **6**, 1021–1024 (2004).
8. Balakrishnan, P. G., Ramesh, R. & Prem Kumar, T. Safety mechanisms in lithium-ion batteries. *J. Power Sources* **155**, 401–414 (2006).
9. Zhang, S. S. A review on the separators of liquid electrolyte Li-ion batteries. *J. Power Sources* **164**, 351–364 (2007).
10. Baginska, M. *et al.* Autonomic shutdown of lithium-ion batteries using thermoresponsive microspheres. *Adv. Energy Mater.* **2**, 583–590 (2012).
11. Choi, J.-A., Kim, S. H. & Kim, D.-W. Enhancement of thermal stability and cycling performance in lithium-ion cells through the use of ceramic-coated separators. *J. Power Sources* **195**, 6192–6196 (2010).
12. Jung, Y. S. *et al.* Improved functionality of lithium-ion batteries enabled by atomic layer deposition on the porous microstructure of polymer separators and coating electrodes. *Adv. Energy Mater.* **2**, 1022–1027 (2012).
13. Feng, J. K., Ai, X. P., Cao, Y. L. & Yang, H. X. Polytriphenylamine used as an electroactive separator material for overcharge protection of rechargeable lithium battery. *J. Power Sources* **161**, 545–549 (2006).
14. Li, S. L., Ai, X. P., Yang, H. X. & Cao, Y. L. A polytriphenylamine-modified separator with reversible overcharge protection for 3.6 V-class lithium-ion battery. *J. Power Sources* **189**, 771–774 (2009).
15. Zhang, H., Cao, Y., Yang, H., Lu, S. & Ai, X. A redox-active polythiophene-modified separator for safety control of lithium-ion batteries. *J. Polym. Sci. B* **51**, 1487–1493 (2013).
16. Hyung, Y. E., Vissers, D. R. & Amine, K. Flame-retardant additives for lithium-ion batteries. *J. Power Sources* **119–121**, 383–387 (2003).
17. Xiang, H. F., Xu, H. Y., Wang, Z. Z. & Chen, C. H. Dimethyl methylphosphonate (DMMP) as an efficient flame retardant additive for the lithium-ion battery electrolytes. *J. Power Sources* **173**, 562–564 (2007).
18. Buhrmester, C. *et al.* Studies of aromatic redox shuttle additives for $LiFePO_4$-based Li-ion cells. *J. Electrochem. Soc.* **152**, A2390–A2399 (2005).
19. Chen, Z., Qin, Y. & Amine, K. Redox shuttles for safer lithium-ion batteries. *Electrochim. Acta* **54**, 5605–5613 (2009).
20. Zhang, L., Zhang, Z., Wu, H. & Amine, K. Novel redox shuttle additive for high-voltage cathode materials. *Energy Environ. Sci.* **4**, 2858–2862 (2011).
21. Zhang, L., Zhang, Z., Redfern, P. C., Curtiss, L. A. & Amine, K. Molecular engineering towards safer lithium-ion batteries: a highly stable and compatible redox shuttle for overcharge protection. *Energy Environ. Sci.* **5**, 8204–8207 (2012).
22. Chen, R.-J., Wu, F., Li, L., Qiu, X.-P. & Chen, S. Binary molten salt electrolytes based on $LiClO_4$ and 2-oxazolidinone. *Acta Phys.-Chim. Sin.* **23**, 554–558 (2007).
23. Xu, K., Zhang, S., Allen, J. L. & Jow, T. R. Nonflammable electrolytes for Li-ion batteries based on a fluorinated phosphate. *J. Electrochem. Soc.* **149**, A1079–A1082 (2002).
24. Wong, D. H. C. *et al.* Nonflammable perfluoropolyether-based electrolytes for lithium batteries. *Proc. Natl Acad. Sci. USA* **111**, 3327–3331 (2014).
25. Zhang, X.-W., Wang, C., Appleby, A. J. & Little, F. E. Characteristics of lithium-ion-conducting composite polymer-glass secondary cell electrolytes. *J. Power Sources* **112**, 209–215 (2002).
26. Ghosh, A., Wang, C. & Kofinas, P. Block copolymer solid battery electrolyte with high Li-ion transference number. *J. Electrochem. Soc.* **157**, A846–A849 (2010).
27. Liu, G., Reinhout, M., Mainguy, B. & Baker, G. L. Synthesis, structure, and ionic conductivity of self-assembled amphiphilic poly(methacrylate) comb polymers. *Macromolecules* **39**, 4726–4734 (2006).
28. Liu, G., Reeder, C. L., Sun, X. & Kerr, J. B. Diffusion coefficients in trimethyleneoxide containing comb branch polymer electrolytes. *Solid State Ion.* **175**, 781–783 (2004).
29. Bouchet, R. *et al.* Single-ion BAB triblock copolymers as highly efficient electrolytes for lithium-metal batteries. *Nature Mater.* **12**, 452–457 (2013).
30. Li, J. *et al.* A positive-temperature-coefficient layer based on Ni-mixed poly(vinylidene fluoride) composites for $LiFePO_4$ electrode. *Int. J. Electrochem. Sci.* **8**, 5223–5231 (2013).
31. Zhou, F., Zhao, X. & Dahn, J. R. Impact of Al or Mg substitution on the thermal Stability of $Li_{1.05}Mn_{1.95-z}M_zO_4$ (M = Al or Mg). *J. Electrochem. Soc.* **157**, A798–A801 (2010).
32. Xia, L., Li, S.-L., Ai, X.-P., Yang, H.-X. & Cao, Y.-L. Temperature-sensitive cathode materials for safer lithium-ion batteries. *Energy Environ. Sci.* **4**, 2845–2848 (2011).
33. Bloor, D., Graham, A., Williams, E. J., Laughlin, P. J. & Lussey, D. Metal–polymer composite with nanostructured filler particles and amplified physical properties. *Appl. Phys. Lett.* **88**, 102103 (2006).
34. Bartenev, G. M., Remizova, A. A., Kuleshov, I. V. & Martynov, M. A. Volume expansion of polyethylene with various degrees of crystallinity over a wide range of temperatures. *Polym. Sci. USSR* **15**, 2808–2813 (1973).
35. Yang, G. F., Song, K. Y. & Joo, S. K. A metal foam as a current collector for high power and high capacity lithium iron phosphate batteries. *J. Mater. Chem. A* **2**, 19648–19652 (2014).
36. Veith, G. M. & Dudney, N. J. Current collectors for rechargeable Li-air batteries. *J. Electrochem. Soc.* **158**, A658–A663 (2011).
37. Nan, C. W., Shen, Y. & Ma, J. Physical properties of composites near percolation. *Annu. Rev. Mater. Res.* **40**, 131–151 (2010).
38. Alvarez, M. P., Poblete, V. H., Pilleux, M. E. & Fuenzalida, V. M. Submicron copper-low-density polyethylene conducting composite-structural electrical and percolation threshold. *J. Appl. Polym. Sci.* **99**, 3005–3008 (2006).
39. Xia, L., Zhu, L., Zhang, H. & Ai, X. A positive-temperature-coefficient electrode with thermal protection mechanism for rechargeable lithium batteries. *Chin. Sci. Bull.* **57**, 4205–4209 (2012).
40. Chen, R. *et al.* Positive temperature coefficient effect of polymer-carbon filler composites under self-heating evaluated quantitatively in terms of potential barrier height and width associated with tunnel current. *Polymer* **53**, 5197–5207 (2012).
41. Wei, D., Zhao, T. & Xiao, S. Y. Resistivity-volume expansion characteristics of carbon black-loaded polyethylene. *J. Appl. Polym. Sci.* **77**, 53–58 (2000).
42. Kono, A. *et al.* Positive-temperature-coefficient effect of electrical resistivity below melting point of poly(vinylidene fluoride) (PVDF) in Ni particle-dispersed PVDF composites. *Polymer* **53**, 1760–1764 (2012).
43. Li, D., Yang, K., Chen, S. & Wu, F. Thermal behavior of overcharged nickel/metal hydride batteries. *J. Power Sources* **184**, 622–626 (2008).
44. Kise, M. *et al.* Development of new safe electrode for lithium rechargeable battery. *J. Power Sources* **146**, 775–778 (2005).
45. Zhong, H., Kong, C., Zhan, H., Zhan, C. & Zhou, Y. Safe positive temperature coefficient composite cathode for lithium ion battery. *J. Power Sources* **216**, 273–280 (2012).
46. Yoon, S.-M. *et al.* Synthesis of multilayer graphene balls by carbon segregation from nickel nanoparticles. *ACS Nano* **6**, 6803–6811 (2012).

Acknowledgements

This work was partially supported by the Department of Energy, Laboratory Directed Research and Development funding, under contract DE-AC02-76-SF00515 and by the Precourt Institute for Energy at Stanford University. We thank K. Yan for discussions and J. Tok for proof reading of the manuscript.

Author contributions

Z.B., Y.C. and Z.C. conceived and designed the experiment. Z.C. carried out materials fabrication, characterization and testing. P.-C.H. conducted COMSOL simulations. J.L. performed DSC measurements. Y.L. conducted the graphene coating for nano-spiky nickel particles. J.W.F.T. and N.L. did the XPS and Raman characterization, respectively. C.W., S.C.A. and J.L. provided constructive advice for the experiment and figure preparation. Z.C. wrote the first draft. Z.B. and Y.C. revised the manuscript. All authors made comments on the paper.

Additional information

Supplementary information is available online. Reprints and permissions information is available online at www.nature.com/reprints. Correspondence and requests for materials should be addressed to Y.C. or Z.B.

Competing interests

The authors declare no competing financial interests.